



Contents lists available at ScienceDirect

Biosensors and Bioelectronics

journal homepage: www.elsevier.com/locate/bios



Slotted photonic crystal cavities with integrated microfluidics for biosensing applications

M.G. Scullion*, A. Di Falco, T.F. Krauss

School of Physics and Astronomy, University of St Andrews, North Haugh, St Andrews, Fife, KY16 9SS, Scotland, UK

ARTICLE INFO

Article history:

Received 24 March 2011
Received in revised form 16 June 2011
Accepted 18 June 2011
Available online xxx

Keywords:

Slot waveguide
Photonic crystal
Slotted photonic crystal
Optical biosensor
Microfluidic

ABSTRACT

We demonstrate the detection of dissolved avidin concentrations as low as 15 nM or 1 µg/ml using functionalized slotted photonic crystal cavities with integrated microfluidics. With a cavity sensing surface area of approximately 2.2 µm², we are able to detect surface mass densities of order 60 pg/mm² corresponding to a bound mass of approximately 100 ag. The ultra-compact size of the sensors makes them attractive for lab-on-a-chip applications where high densities of independent sensing elements are desired within a small area. The high sensitivity over an extremely small area is due to the strong modal overlap with the analyte enabled by the slotted waveguide cavity geometry that we employ. This strong overlap results in larger shifts in the cavity peak wavelength when compared to competing approaches.

© 2011 Elsevier B.V. All rights reserved.

1. Introduction

Small integrated optical biosensors (Fan et al., 2008), such as surface plasmon (Homola, 2008), photonic crystal (Cunningham, 2010; Lee and Fauchet, 2007a,b; Mandal et al., 2009; Skivesen et al., 2007; Toccafondo et al., 2010) and ring resonator (De Vos et al., 2007; Ksendov and Lin, 2005; Li and Fan, 2010) based devices, are the subject of an intense research effort in the lab-on-a-chip community. Many of these devices can be designed to operate 'label-free', thus eliminating the need for fluorescent labels and greatly reducing the time, skill and effort involved for the user (Fan et al., 2008). Slotted photonic crystals (SPhC) (Di Falco et al., 2008a,b; Yamamoto et al., 2008) have gained attention in this field due to the greatly enhanced light-matter interaction they offer. Such devices combine the spatial confinement of the optical field provided by slot waveguides (Almeida et al., 2004; Xu et al., 2004) (which are also used for sensing purposes (Barrios et al., 2007; Barrios, 2009; Carlborg et al., 2010)), with the temporal confinement provided by photonic crystal cavities, resulting in strong overlap of optical field with the contents of a narrow air slot. This ability to use the peak of the optical mode, rather than the evanescent tail that is typically used in other devices, has resulted in slotted photonic crystals being used for chemical (Di Falco et al., 2009; Kwon et al., 2008) and gas (Jagerska et al., 2010) sensing with high sensitivity, even though the structures are only micron-size in length. Whilst these

devices allow the measurement of very small changes in refractive index, they have no specificity when the analyte composition is unknown, so antibody-antigen binding is used to enable discrimination between different types of proteins (Byrne et al., 2009). As an example, we use cavities functionalised with biotin to demonstrate the detection of avidin, a commonly used technique in biological assays and a good model system for comparison with competing approaches (Lapin and Chabal, 2009; Wilchek et al., 2006). Whilst this particular assay is chosen here as a proof-of-principle demonstration, the device could also be useful for detecting other proteins when functionalized with appropriate antibodies. The very small footprint of our devices and the use of microfluidic channels offer the prospect for high levels of integration with tens or even hundreds of independent sensor elements on a very small footprint, thus enabling multi-functionality and multimodal detection.

2. Materials and methods

2.1. Device principles and fabrication

To improve the interaction between the analyte in the slot and the incident light, high quality factor cavities can be constructed with photonic crystals. The spectral position of the cavity also provides a well-defined point of reference in the transmission spectrum of the device allowing direct inference of the refractive index of the analyte. Our cavities, previously reported in (Di Falco et al., 2009), are constructed using the heterostructure approach (Akahane et al., 2003; Song et al., 2005) by locally compressing the lattice constant of the crystal around 3 columns of holes in the

* Corresponding author.

E-mail address: mgs32@st-andrews.ac.uk (M.G. Scullion).

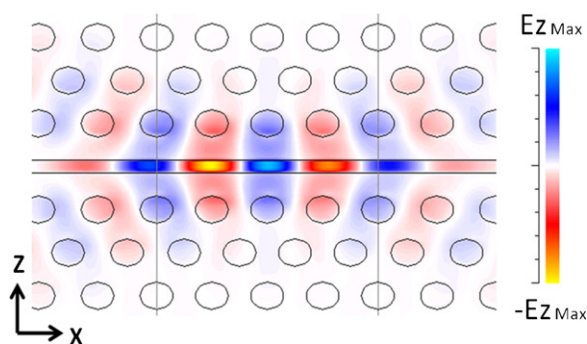


Fig. 1. 2D FDTD simulation of slotted photonic crystal air cavity showing E_z component of mode profile at cavity resonant wavelength. Period 490 nm, cavity period 460 nm, hole radius 135 nm and slot width 120 nm. Vertical lines show cavity boundaries.

centre of the crystal. The result of a 2D FDTD simulation of an air slot photonic crystal cavity is shown in Fig. 1 (period 490 nm, cavity period 460 nm, hole radius 135 nm and slot width 120 nm) to illustrate the mode profile of the device and highlight the large overlap of the mode with the analyte that gives rise to the high figure of merit ($d\lambda/dn$) that we observe with these devices. The simulation was run with slab effective index 2.7, background index 1.0, electric field parallel to the PhC plane, free space wavelength 1700 nm and 0.4 nm spectral resolution. It should be noted that the cavity peak wavelength has a strong dependence on the slot width used in both experiment and theory, and changes in the slot contents cause a significant shift in the cavity operational wavelength (Di Falco et al., 2009). Quality factors of 50,000 in air (70,000 theoretical) and 4000 (6000 theoretical) in water have been demonstrated using this design, with bulk refractive index sensitivity values of up to 1500 nm/RIU (Di Falco et al., 2009). Here, we detect changes in the refractive index at the surface of the device. Biotin receptors are attached to the surface using amine chemistry, enabling the specific detection of dissolved avidin. As avidin binds to the biotin on the surface of the slot cavity, the local refractive index at the surface changes resulting in a shift of the cavity peak wavelength that can be tracked in real time. Cavities are designed to operate around the telecommunications window of 1550 nm where there is a slight dip in the water absorption spectrum (De Vos et al., 2007), and where many optical sources and detectors are available. We utilise resonant defects at the sample edge to improve coupling efficiency into the slotted photonic crystal (Scullion et al., 2011).

The structures were created in silicon-on-insulator (SOI) substrates (220 nm thick top layer) using electron beam lithography, reactive ion etching and hydrofluoric acid under-etching as detailed in (Di Falco et al., 2008a, 2009). We chose silicon for our photonic crystals because of its optical performance and established manufacturing processes, but most importantly, for its high refractive index, which is necessary for the strong modal confinement in the slot and the high Q -factor cavities. This strong confinement is essential for achieving the high figure of merit ($d\lambda/dn$) and would not be available with low-index platforms, such as organic polymers. A triangular lattice of holes of period 490 nm and radius 135 nm was used, with a cavity defect period of 460 nm and a slot width of 120 nm. SEM images of the device are shown in Fig. 2.

Poly(dimethylsiloxane) (PDMS) microfluidic structures were created using SU-8 moulds and soft lithography (Xia and Whitesides, 1998). SU-8 photoresist (Microchem, 1 part 2000.5 to 10 parts 2050) was spun to a thickness of 40 μm on a piece of silicon wafer and pre-baked at 65 °C for 5 min and 95 °C for 15 min on a hotplate. The pre-baked sample was then exposed to UV through a photomask of the channel design in a mask aligner for 2 min, before removing and post-baking at 65 °C for 1 min and 95 °C for 10 min.

The sample was then developed in EC solvent and rinsed in IPA. The final mould was hard-baked overnight in a 180 °C oven. Channel widths of approximately 200 μm were used. Sylgard 184 PDMS base and curing agent were mixed in a ratio of 10:1 by weight and degassed in a dessicator. The liquid was then poured over the SU-8 mould inside a petri dish, and left in a 65 °C oven for over 4 h. The solidified PDMS was then carefully peeled from the mould, cut to size with a small blade, and two 2 mm access holes punched through from the channel ends to the top surface.

Before bonding the microfluidics on top, the SOI containing the SPHCs was first immersed in Piranha solution (1 part hydrogen peroxide to 3 parts sulphuric acid) for 30 min to ensure the surface was thoroughly clean, and to form a thin layer of oxide that is used to aid antibody attachment during functionalization. The bottom layer of the PDMS microfluidic chip was then exposed to oxygen plasma using a handheld coronal discharge gun, exposing free hydroxyl bonds. Using methanol as a lubricant, the PDMS chip was placed on top of the SOI, and the microchannel aligned to the photonic crystals under an optical microscope. This step should be completed within a minute or two after exposing the PDMS to plasma to ensure high bonding strength. The aligned chip was carefully placed inside a 65 °C oven and left overnight for the PDMS to chemically bond to the SOI. Pictures and a schematic of the final chip layout are shown in Fig. 3. The chip was then removed and attached to a glass sample holder using silver conductive paint. Rubber tubes of 2.4 mm diameter were compressed into the access holes in the PDMS to allow injection and removal of fluid from the microchannel using a connected syringe.

2.2. Functionalization

A protocol similar to (De Vos et al., 2007; Lapin and Chabal, 2009) was followed to attach biotin molecules to the oxidised SOI, and was carried out entirely within the bonded PDMS microfluidic channel. Aminopropyltriethoxysilane (APTES) was diluted in 95% ethanol to a concentration of 2% and injected into the microchannel using a syringe connected to the inlet tubing. Ethanol was chosen to provide compatibility with the PDMS structures, which swell in strong organic solvents (Lee et al., 2003). The APTES solution was left inside the channel overnight (19 h in total) to allow aminosilination of the surface, which enables biotin surface immobilization (Lapin and Chabal, 2009). The channel was then flushed with ethanol and deionised water several times and cured inside a 65 °C oven for over 5 h. Biotinamidohexanoic acid N-hydroxysuccinimide (NHS-linked biotin) ester powder (Sigma–Aldrich, UK) was dissolved in dimethylformamide (DMF) to a concentration of 1 mg/ml. 200 μl of this solution was then added to 2 ml of phosphate buffered saline (PBS) solution. This biotin/DMF/PBS solution was injected into the chip after curing, and left for over 12 h inside the channel. The sample was then flushed several times with PBS before the sensor was ready to accept avidin.

2.3. Optical characterization

Light from a broadband ASE source (1525–1620 nm, output power 50 mW) was sent from a fibre into a collimating lens and through a TE polariser before being focused onto the sample edge using a 60 \times objective (see Fig. 3a). Waveguide input and output spots were observed using a 20 \times objective and infra-red camera from above. Light from the output of a waveguide was then collected by a 40 \times lens and sent to a single mode fibre, before being split between an optical spectral analyser (OSA) and a photodetector. Once aligned, the chemicals were passed through the microchannel to functionalize the surface as outlined above. The OSA was used to track changes in the output spectrum.

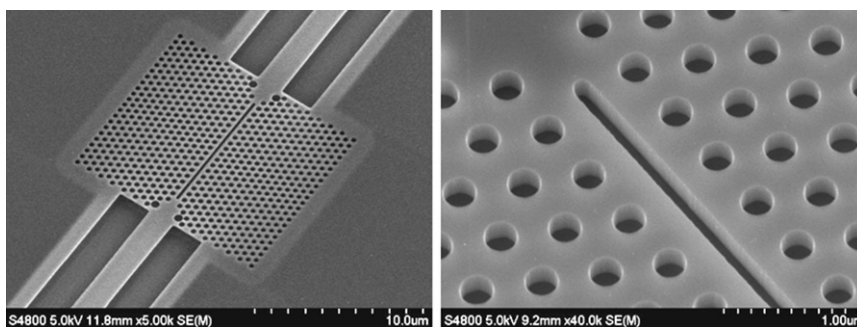


Fig. 2. SEM images of slotted photonic crystal cavities fabricated in SOL.

3. Results

Avidin solutions of varying concentration were created by serially diluting avidin from egg-white lyophilized powder (Sigma–Aldrich, UK) from 100 $\mu\text{g}/\text{ml}$ down to 1 ng/ml in PBS. Pure PBS was first injected by syringe into the inlet tube and a reference spectrum taken. Avidin solutions of increasing concentration were then injected and left to sit within the microchannel, rather than continually flowed through. Measurements of the slotted photonic crystal spectrum were taken every minute, for typically 30 min, before the next concentration was introduced. A pure PBS solution was injected at the end for final reference. The full experiment is shown in Fig. 4, which depicts the variation in the cavity peak wavelength with time based on a Lorentzian fit. Each dotted line represents the point at which the next concentration of avidin solution was injected. Movement is observed at all concentrations, but the first clearest positive shift occurs at a concentration of 1 $\mu\text{g}/\text{ml}$. At higher concentrations it can be observed within Fig. 4 that each injection causes the peak to drop to a shorter wavelength before continuing to rise. This occurs as the sensing surface approaches saturation, with each injection displacing avidin molecules that

have not properly bonded to biotin (Carlborg et al., 2010). The final PBS flush also continues to rise after flushing, possibly due to weak reattachment of unbound material within the slot. Note again that the solution is left to sit within the channel, rather than continually flowed through, thus material displaced by an initial flush can settle back into the slot. A better measure of the bound mass is therefore the point just after flushing each concentration (the dips in Fig. 4), rather than the maximum peak shift for a given concentration. The inset in Fig. 4 depicts the variation in cavity peak wavelength with concentration at each of these points. Fig. 5 shows the actual peaks at each concentration. The Q -value of these peaks is approximately 3000, and we here comfortably measure shifts in wavelength of greater than 0.1 nm.

4. Discussion

The unambiguously measurable detection limit for avidin here is 1 $\mu\text{g}/\text{ml}$. As avidin molecules have a molecular weight of 68 kDa (Green, 1964), this corresponds to a molar concentration of 15 nM. This concentration is reasonably close to or better than other small optical sensors (Lee and Fauchet, 2007a,b; Li and Fan, 2010; Mandal

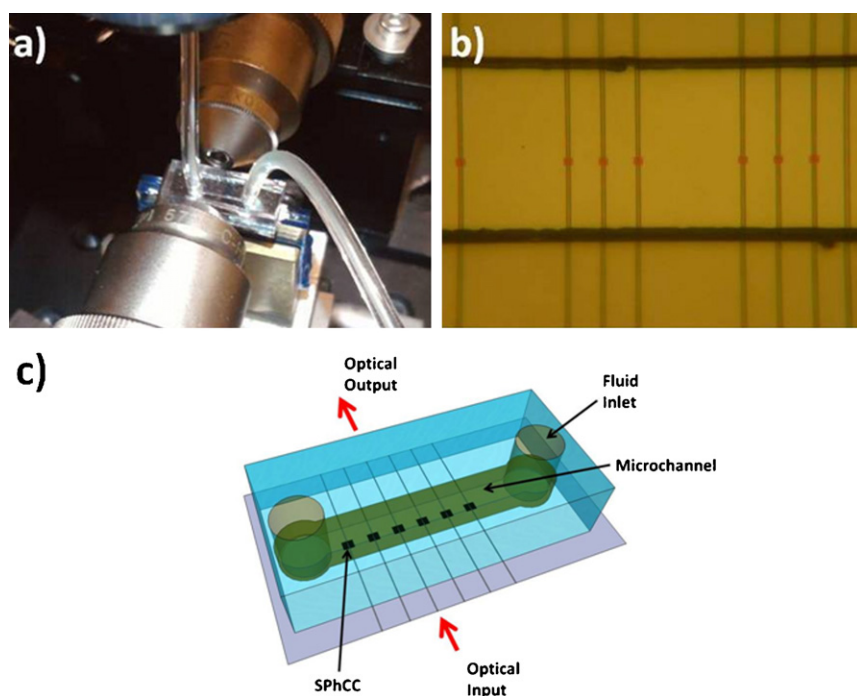


Fig. 3. (a) Aligned sensor chip with connected tubes for fluid injection. (b) Top view of bonded PDMS microfluidic channel (200 μm wide, 40 μm high) with SPhC (10 $\mu\text{m} \times 13 \mu\text{m}$) inside. (c) Schematic of slotted photonic crystal sensors with integrated PDMS microfluidics (not to scale).

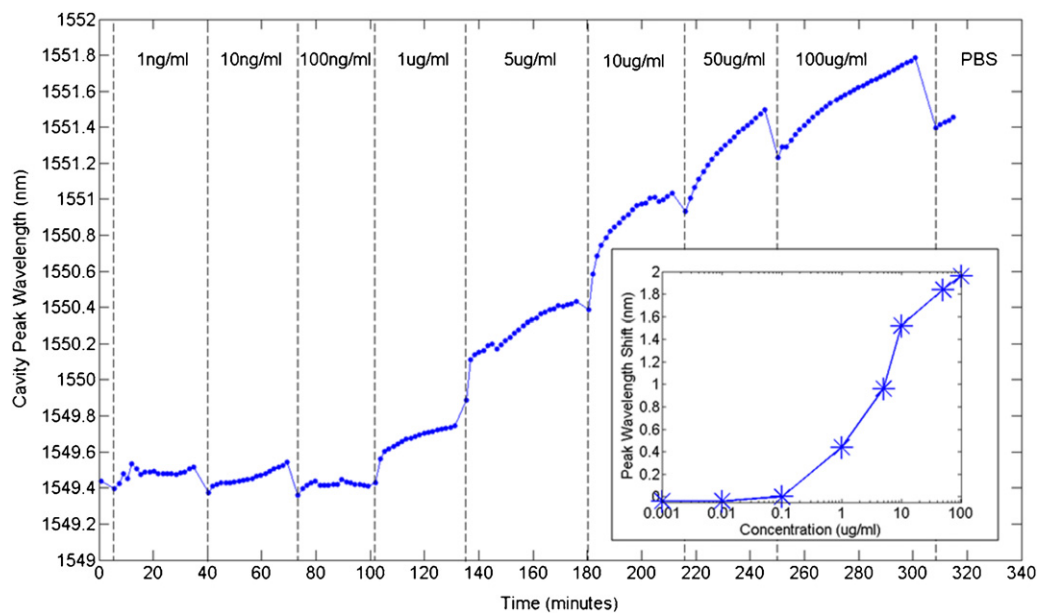


Fig. 4. Real time measurements of avidin/biotin binding showing variation in cavity peak wavelength (based on Lorentzian fit) with time for several avidin concentrations. Inset: cavity peak wavelength shift from starting position as a function of avidin concentration in PBS. Values correspond to those taken just after flushing each concentration.

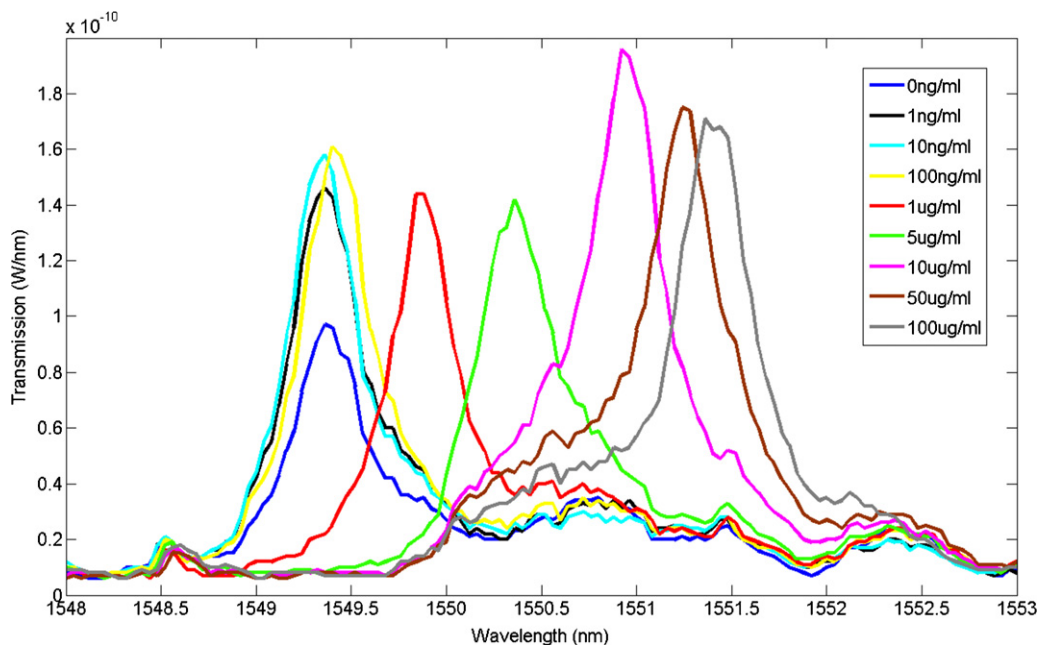


Fig. 5. Cavity peaks recorded at each concentration of dissolved avidin.

Table 1
 Comparison of small optical biosensors.

Reference	Peak wavelength shift for 10 $\mu\text{g/ml}$ conc. (nm)	Estimated sensing surface area (μm^2)	Minimum conc. detected ($\mu\text{g/ml}$)
Our work	1.5	2.2	1
Barrios et al. (2007), Barrios (2009)	2.5	>250	0.042
Carlborg et al. (2010)	1.2	>250	0.125
De Vos et al. (2007)	0.55	21.8	0.01
Lee and Fauchet (2007a,b)	-	50	2%
Li and Fan (2010)	0.001	>250	10 nM
Mandal et al. (2009)	0.25	8.36	1
Skivesen et al. (2007)	0.2	>100	10
Toccafondo et al. (2010)	<0.2	>100	19.8 nM

et al., 2009; Skivesen et al., 2007; Toccafondo et al., 2010) despite the sensing area being significantly smaller, which highlights the benefit of using the slotted photonic crystal geometry. In addition, our device has a footprint of $10\ \mu\text{m} \times 13\ \mu\text{m}$ and a sensing area of only $\approx 2\ \mu\text{m}^2$. In comparison to other devices, such as those based on slotted or conventional ring resonators, the performance is remarkable for a device so small. Peak wavelength shifts at a concentration of $10\ \mu\text{g/ml}$ ($150\ \text{nM}$) are significantly larger than comparable devices, as shown in Table 1. We detect a larger shift for this concentration due to the stronger interaction between the optical mode and analyte resulting from the slot cavity architecture. The only devices with higher performance in terms of detecting smaller concentrations have a significantly larger sensing surface area, $21.8\ \mu\text{m}^2$ in (De Vos et al., 2007) and $>250\ \mu\text{m}^2$ in (Barrios et al., 2007; Barrios, 2009; Carlborg et al., 2010) compared to our $2\ \mu\text{m}^2$. The real advantage of the photonic crystal slotted geometry is therefore the ability to pack tens or even hundreds of independent sensor elements into the same area, thus allowing impressive multi-functionality in a very small device. Potentially, each sensor in an array could be functionalized to detect different proteins using nanometre precision direct writing techniques such as dip-pen nanolithography (Piner et al., 1999), thus reducing the amount of analyte required to run multiple tests. A further advantage of our geometry compared to, for example, ring-resonator based sensors, is that our cavities exhibit a large free spectral range. This allows for large (10^3 – 10^4) arrays to be multiplexed on the same chip, each exhibiting a unique resonance frequency.

The surface density σ_p of biomolecules bound to the sensing area when observing the smallest clear wavelength shift $\delta\lambda$ can be estimated using the equation (White and Fan, 2008):

$$\frac{\delta\lambda}{\lambda} = \sigma_p \alpha_{\text{ex}} \frac{2\pi \sqrt{n_m^2 - n_s^2} n_m}{\epsilon_0 \lambda^2 n_s^2} S \quad (1)$$

where α_{ex} is the excess polarizability of the molecule, n_m is the refractive index of the sensor material, n_s is the refractive index of the analyte and S is the bulk refractive index sensitivity of the sensor. Given our values of $500\ \text{nm/RIU}$ (theoretical) (Di Falco et al., 2009) for the bulk sensitivity, $n_m = 3.4$ (silicon), $n_s = 1.35$ (PBS), $\lambda = 1550\ \text{nm}$, $\delta\lambda \approx 0.4\ \text{nm}$ (the shift we detect at $1\ \mu\text{g/ml}$) and $\alpha_{\text{ex}} = 4\pi\epsilon_0(3.2 \times 10^{-21})\ \text{cm}^3$ (Arnold et al., 2003; Boleininger et al., 2010), the surface density is found to be 5×10^8 molecules/ mm^2 , which corresponds to a surface mass density of $60\ \text{pg/mm}^2$. Based on FDTD simulations of the cavity (see Fig. 1) we estimate the surface area involved in sensing to be as low as $2.2\ \mu\text{m}^2$. Given this value we expect the amount of detectable bound mass to be around $100\ \text{ag}$. We note, however, the inherent uncertainties in the above estimations at such low mass levels, so only quote this figure for comparison to other devices in the published literature. Although the biotin solution is left in contact with the surface for over 12 h, sensitivity and avoidance of non-specific binding could be improved by adding blocking agents to the protocol we follow (De Vos et al., 2007). The specificity of avidin/biotin binding has already been established for this protocol (De Vos et al., 2007; Lapin and Chabal, 2009).

Detection of concentrations below $15\ \text{nM}$ could possibly be achieved using higher quality factor cavities, a pump to constantly replenish the available target proteins passing over the sensor and by waiting for significantly longer periods of time than the 30 min used here. Cavities operating at $1550\ \text{nm}$ are limited in their quality factor Q by the low refractive index contrast and water absorption, in our case to around $Q \approx 6000$. Shifting to the $1300\ \text{nm}$ window should improve the Q due to the reduction in water absorption by more than an order of magnitude, thus allowing smaller shifts to be

detected. The use of very high Q -factors, however, carries the added problems of increased uncertainty due to effects such as thermal noise.

5. Conclusion

We have designed, fabricated and tested a novel functionalized slotted photonic crystal cavity with integrated microfluidic circuitry, and demonstrated its use for biochemical sensing. Using biotin as a receptor, we detect concentrations of dissolved avidin as low as $15\ \text{nM}$. Given that the actual sensing area used is $2.2\ \mu\text{m}^2$, this is impressive when compared with much larger devices, and results in figures of $60\ \text{pg/mm}^2$ and $100\ \text{ag}$ for the detectable mass density and bound mass respectively. Based on these results, we expect to detect protein masses well below the femtogram levels within the cavity. With the appropriate choice of antibody, the sensor could be adapted to detect other proteins. The small size of the device, combined with our successful implementation of functionalization within bonded microfluidic channels suggests a strong potential for large arrays of independent sensors on centimetre sized chips.

Acknowledgements

ADF is supported by an EPSRC Career Acceleration Fellowship (EP/I004602/1). We also appreciate support from EPSRC under grant no. EP/F020589/1.

References

- Akahane, Y., Asano, T., Song, B.S., Noda, S., 2003. *Nature* 425, 944–947.
- Almeida, V.R., Xu, Q., Barrios, C.A., Lipson, M., 2004. *Opt. Lett.* 29, 1209–1211.
- Arnold, S., Khoshshima, M., Teraoka, I., Holler, S., Vollmer, F., 2003. *Opt. Lett.* 28, 272–274.
- Barrios, C.A., Gylfason, K.B., Sanchez, B., Griol, A., Sohlstrom, H., Holgado, M., Casquel, R., 2007. *Opt. Lett.* 32, 3080–3082.
- Barrios, C.A., 2009. *Sensors* 9, 4751–4765.
- Boleininger, A., Lake, T., Hami, S., Vallance, C., 2010. *Sensors* 10, 1765–1781.
- Byrne, B., Stack, E., Gilmartin, N., O'Kennedy, R., 2009. *Sensors* 9, 4407–4445.
- Cunningham, B.T., 2010. *JALA* 15, 120–135.
- Carlborg, C.F., Gylfason, K.B., Kazmierczak, A., Dortu, F., Banuls Polo, M.J., Maquieira Catala, A., Kresbach, G.M., Sohlstrom, H., Moh, T., Vivien, L., Popplewell, J., Ronan, G., Barrios, C.A., Stemme, G., Van der Wijngaert, W., 2010. *Lab Chip* 10, 281–290.
- De Vos, K., Bartolozzi, I., Scaht, E., Bienstman, P., Baets, R., 2007. *Opt. Express* 15, 7610–7615.
- Di Falco, A., O'Faolain, L., Krauss, T.F., 2008a. *Phot. Nan. Fun. Appl.* 6, 38–41.
- Di Falco, A., O'Faolain, L., Krauss, T.F., 2008b. *Appl. Phys. Lett.* 92, 083501.
- Di Falco, A., O'Faolain, L., Krauss, T.F., 2009. *Appl. Phys. Lett.* 94, 063503.
- Fan, X., White, I., Shopova, S.I., Zhu, H., Suter, J.D., Sun, Y., 2008. *Anal. Chim. Acta* 620, 8–26.
- Green, N.M., 1964. *Biochem. J.* 92, 16–17.
- Homola, J., 2008. *Chem. Rev.* 108, 462–493.
- Jagerska, J., Zhang, H., Diao, Z., Le Thomas, N., Houdre, R., 2010. *Opt. Lett.* 35, 2523–2525.
- Ksendov, A., Lin, Y., 2005. *Opt. Lett.* 30, 3344–3346.
- Kwon, S.H., Sunner, T., Kamp, M., Forchel, A., 2008. *Opt. Express* 16, 11709–11717.
- Lapin, N.A., Chabal, Y.J., 2009. *J. Phys. Chem. B* 113, 8776–8783.
- Lee, J.N., Park, C., Whitesides, G.M., 2003. *Anal. Chem.* 75, 6544–6554.
- Lee, M., Fauchet, P.M., 2007a. *Opt. Express* 15, 4530–4535.
- Lee, M., Fauchet, P.M., 2007b. *Opt. Lett.* 32, 3284–3286.
- Li, H., Fan, X., 2010. *Appl. Phys. Lett.* 97, 011105.
- Mandal, S., Goddard, J.M., Erickson, D., 2009. *Lab Chip* 9, 2924–2932.
- Piner, R.D., Zhu, J., Xu, F., Hong, S., Mirkin, C.A., 1999. *Science* 283, 661–663.
- Scullion, M.G., Krauss, T.F., Di Falco, A., 2011. *IEEE J. Photonics* 3, 203–208.
- Skivesen, N., Tetu, A., Kristensen, M., Kjems, J., Frandsen, L.H., Borel, P.I., 2007. *Opt. Express* 15, 3169–3176.
- Song, B.S., Noda, S., Asano, T., Akahane, Y., 2005. *Nat. Mater.* 4, 207–210.
- Toccafondo, V., Garcia-Ruperez, J., Banuls, M.J., Griol, A., Castello, J.G., Perans-Llopi, S., Maquieira, A., 2010. *Opt. Lett.* 35, 3673–3675.
- White, I.M., Fan, X., 2008. *Opt. Express* 16, 1020–1028.
- Wilchek, M., Bayer, E.A., Livnah, O., 2006. *Immunol. Lett.* 103, 27–32.
- Xia, Y., Whitesides, G.M., 1998. *Annu. Rev. Mater. Sci.* 28, 153–184.
- Xu, Q., Almeida, V.R., Panepucci, R.R., Lipson, M., 2004. *Opt. Lett.* 29, 1626–1628.
- Yamamoto, T., Notomi, M., Taniyama, H., Kuramochi, E., Yoshikawa, Y., Torii, Y., Kuga, T., 2008. *Opt. Express* 16, 13809–13817.